MIT Libraries | DSpace@MIT

MIT Open Access Articles

Increased Natural Ventilation Flow Rates through Ventilation Shafts

Massachusetts Institute of Technology

Increased Natural Ventilation Flow Rates through Ventilation Shafts

Stephen D. Ray[+]
Leon R. Glicksman

Building Technology Program, MIT
77 Massachusetts Ave Rm. 5-418 Cambridge MA, USA
[+] Corresponding author - sdray@mit.edu

Abstract

Buoyancy-driven natural ventilation in ventilation shafts is investigated with a small scale physical experiment within a duct and CFD simulations of an office building. For a fixed exhaust opening, smaller shafts lead to higher flow rates in upper floors of a multi-story building with a shared ventilation shaft. These higher flow rates are caused by increased vertical momentum within the smaller shafts that induce flow through upper floors, an effect referred to as the "ejector effect." In the small scale duct, a 0.5 m by 0.5 m shaft leads to a slight reverse flow of 0.0029 m^3/s through the upper floor. Holding all other parameters constant and reducing the shaft to 0.25 m by 0.5 m leads to a positive flow rate of 0.012 m^3/s through the upper floor. In the CFD simulations of a three story office building, this same pattern is observed. A 3 m by 2 m shaft leads to a flow rate of 0.0168 m^3/s through the third floor, while the reduced shaft of 2 m by 2 m leads to a flow rate of 0.766 m^3/s through the same floor. This increased airflow rate from the ejector effect can allow natural ventilation to be used in buildings where it may otherwise have been deemed inappropriate. Most airflow network models neglect air momentum and fail to account for the ejector effect. To improve these models, an empirical model is incorporated into the airflow network model CoolVent in a manner easily transferable to most airflow network models.

Keywords: Natural Ventilation, CFD, Atria, Airflow network model, Building simulation

1. Introduction

Natural ventilation is increasingly considered as an alternative to mechanical cooling because of its potential for significant energy savings. Buoyancy-driven natural ventilation leverages the temperature difference between the indoor and outdoor environments to draw outdoor air into buildings. One limitation of buoyancy-driven systems is their requirement that each floor must be connected to an exhaust opening generally located on the roof. Multiple floors are often connected to a common pathway that leads to the exhaust opening. Large atria can provide this pathway as demonstrated in recent research on the Center for Education at the Green Building [1], Houghton Hall [2][3], and the Engineering Building at Concordia University [4]. However, atria require large amounts of indoor space that could otherwise be occupied. To reduce the required footprint of these air pathways, ventilation shafts can be used as demonstrated in recent research on the Hulic Headquarters building [5], the San Diego New Children's Museum [6], the Harm A. Weber Academic Center at Judson College [7], and the School of Slavonic and East European Studies at University College London [8].

When designing buoyancy-driven natural ventilation systems, engineers and architects use various computational tools. Simple analytical models use fundamental equations of heat transfer and fluid dynamics with simplified geometries and boundary conditions to obtain a closed-form solution [9]. However, their simplifications limit their use in designing full scale systems. Computational fluid dynamics (CFD) is commonly used to aid in the

design of buoyancy-driven natural ventilation systems because of its validated accuracy of modeling arbitrary geometries [9]. While very useful in the later stages of design when geometries are well defined, CFD models are not as useful in the early design stages when geometries are not yet well defined. Furthermore, the computational intensity of CFD models limits their use in annual building simulations. Airflow network models divide a building into various nodes that are connected to comprise a network. Fundamental equations of heat transfer and fluid dynamics are applied to the nodes, which are connected in various configurations based on the building design [9]. Airflow rates between zones are typically calculated with a power-law function. Airflow network models can provide annual predictions of natural ventilation system performance, especially when coupled with whole building simulation tools like Energy Plus, TRNSYS, or ESP-r [10-12]. Their applicability can be limited, though, when momentum effects within the space are significant because of their disregard for momentum within each node. In many cases, this assumption of negligible momentum is justified because the typical open-plan office or atrium is large enough that local velocities are small, thereby resulting in very little momentum. However, the smaller cross sectional areas in ventilation shafts lead to moderate velocities, which in turn generate non-trivial momentum. Thus, current airflow network models that neglect momentum inaccurately model ventilation shafts where momentum effects can be important.

This study observes and simulates the airflow within ventilation shafts connected to multiple floors to investigate if, for a given exhaust area, smaller ventilation shafts lead to higher flow rates through upper floors. This effect is referred to as the "ejector effect." Small scale lab experiments within a custom duct and CFD simulations of an office building are used to explore this effect. Additionally, an airflow network model, CoolVent, is enhanced to account for the ejector effect with methods easily transferable to most airflow network models [13]. The improved CoolVent is used to simulate the same office building modeled with CFD to validate the enhancements.

2. Methods

2.1 Small Scale Experiment Investigation

A small scale model of a ventilation shaft is constructed out of 0.79 mm stainless steel ducts surrounded by 5.1 cm of extruded polystyrene insulation with a thermal resistance of 1.8 m^2K/W. One side of the shaft is cut out and replaced with transparent 2.4 mm acrylic sheets to provide a view into the shaft. The inside of the shaft is lined with 1.6 mm black felt to enhance flow visualization techniques. Two shaft configurations are investigated: a 0.25 m x 0.5 m shaft and a 0.5 m by 0.5 m shaft, both of which are shown in Fig. 1. Three takeoff ducts are connected to a common shaft in each configuration. Each of the takeoff ducts contains a resistance heater measuring 25 cm by 15 cm by approximately 2 mm thick used to create a temperature difference between the shaft and ambient conditions, which simulates internal heat gains in a building. Although identical heaters are used, their measured power output slightly differs and is found to be 150, 146, 144 +/- 2.6 W for the lower, middle, and upper takeoff ducts respectively. Using the chimney shaft height as the characteristic length and the measured bulk temperature difference of 4.5 °C, the Grashof number for the system is 1.6 X 10^{10}, which surpasses the proposed similarity threshold provided by Etheridge and Sandberg and used by other small scale natural ventilation studies [1][3][14][15]. Although this small scale experiment does not replicate any other geometries considered in this study, it provides a physical demonstration of the ejector effect.
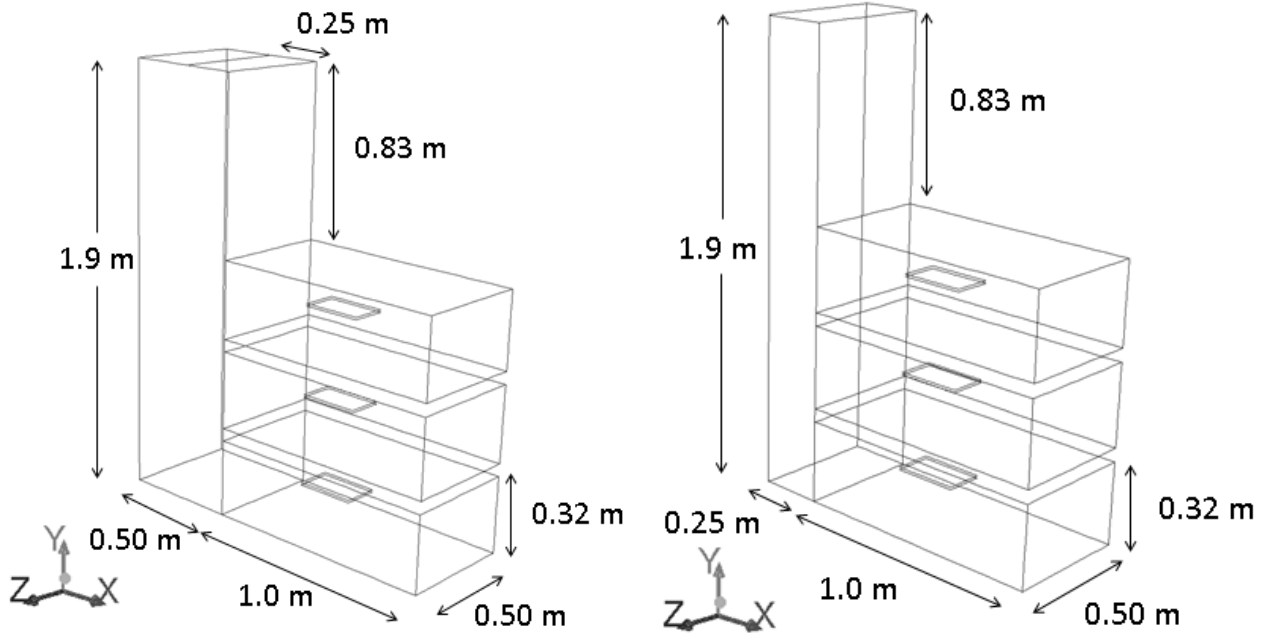
Figure 1 – Geometry of the ventilation shaft lab experiment. Both (left) a 0.5 m by 0.5 m shaft and (right) a 0.25 m by 0.5 m shaft are considered. The three horizontal takeoff ducts are open at both ends so that air enters each duct, is heated by a rectangular heater, and enters the ventilation shaft.

Volumetric flow rates are measured at each inlet in accordance with ASHRAE Standard 111-2008 using the equal area method for the entrance to a rectangular duct [16]. Measurements are made during three tests using a hotwire anemometer with a stated accuracy of +/- 3% +/- 0.015 m/s and are taken flush with the inlets [17]. Airflow visualization is provided by neutrally buoyant bubbles with diameters between 1.3 to 3.8 mm photographed by a digital SLR camera with a shutter speed of 1/4 s to create streaks that correspond to bubble pathlines. The bubble generator is described in more detail elsewhere [18][19].

2.2 CFD Investigation

A CFD investigation is conducted to explore the impact of the ejector effect in a full scale building. Each floor of the three story office building measures 10 m by 10 m by 4 m high, but a 1 m drop ceiling limits the floor-to-ceiling height to 3 m. The floors are naturally ventilated through a single ventilation shaft that extends 4 m above the third floor. A narrow 1 m^2 opening flush with the ceiling on the façade opposite the shaft allows outdoor air to enter the space. Floor-to-ceiling openings from the occupied zone to the shaft allow air to enter the shaft and exit through the 2 m by 2 m exhaust opening at the top of the shaft. Internal heat gains from occupants, lighting, and plug loads are assumed to equal 30 W/m^2. All parameters are held constant except the shaft cross sectional area.

The RNG k-ε turbulence model with enhanced wall function and thermal effects is used based on its computational time and accuracy reported in previous studies [20-25]. Grid independence tests indicate mesh

sizes between 400,295 and 577,697 are sufficient for grid independence, where larger mesh sizes correspond to larger shafts. Mesh density is increased near the narrow opening, floor-to-ceiling opening on each floor, and exhaust opening. Heat loads are evenly distributed across the ceiling and floor. Simulations are run under transient conditions, but are assumed to reach steady state when the bulk exhaust temperature varies less than 0.003 °C for 1000 iterations. Radiation is accounted for using the Surface to Surface radiation model with a residual convergence criteria of 0.001. Reference and operating temperatures are set to 21.8 °C.

An adiabatic boundary condition is applied to all exterior surfaces except the narrow openings, exhaust opening at the top of the shaft, and the floor and ceiling of the occupied zones. The narrow openings are modeled with a "pressure outlet" condition with zero gauge pressure and a specified temperature of 21.8 °C. This condition allows the CFD software to calculate the driving pressure and resulting flow rate due to buoyancy effects from the internal heat gains rather than specifying a flow rate at each opening. A "porous jump" is modeled just inside the narrow opening to account for resistances due to the sudden convergence of the ambient air as it enters the opening. The pressure loss over the "porous jump" is calculated with Eq. 1 where ΔP is the total pressure drop through the "porous jump," ρ is the density of air, v is the local bulk velocity of air, and ζ is the pressure loss coefficient for which a value of 0.5 is used for converging flow [26].

$$\Delta P = \tfrac{1}{2}\zeta\rho v^2 \tag{1}$$

The exhaust opening at the top of the chimney is also modeled with a "pressure outlet" condition. The same "porous jump" condition is applied directly beneath the exhaust opening, but ζ=1 to account for the sudden expansion of the air into the environment after it exits the opening. The floor and ceiling are used to evenly distribute the total heat generation of 30 W/m^2 using a constant heat flux boundary condition.

Five shaft cross-sectional areas are considered: 2 m by 2 m, 2 m by 2.5 m, 2 m by 3 m, 2 m by 3.5 m, and 10 m by 10 m, the last of which models a large atrium. The total exhaust area is 4 m^2 in all five simulations and the exact geometry remains unchanged in the first four simulations. The large atrium case is exhausted by four 1 m^2 openings in the middle of the atrium. In the first four cases, the opening from each floor to the shaft is 6 m^2, while the same opening in the atrium case is 30 m^2. The exact geometry used for three cases is presented in Fig. 2.
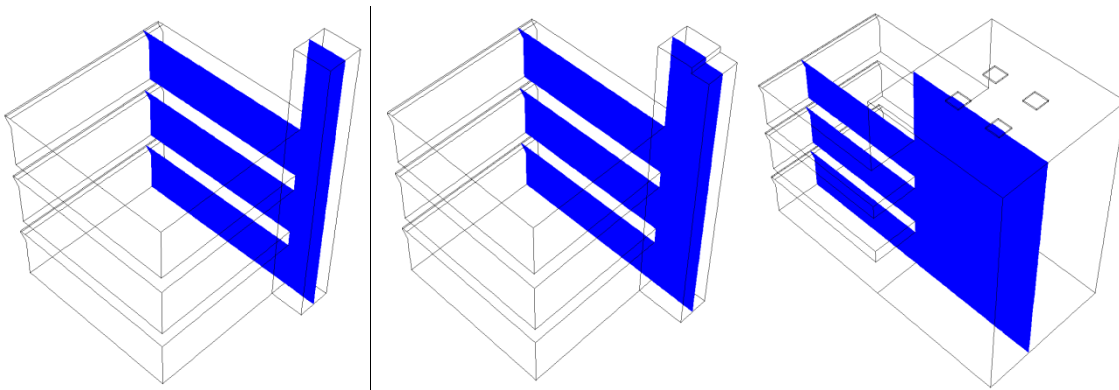
Figure 2 – Basic geometry of the three story office building simulated with CFD. (left) The 2 m by 2 m shaft is expanded to three other cross sections, only one of which is shown, the 2 m by 3 m case (middle). (right) A 10 m by 10 m atrium is also simulated. Every case has the same total exhaust area of 4 m². The blue plane indicates where simulated measurements, which are later presented, are made.

3. Calculations

Following the investigations, an airflow network model, CoolVent, is enhanced to capture the impact of the ejector effect. CoolVent couples the conservation of energy and momentum through numerical methods [13]. Like most airflow network models, CoolVent assumes well-mixed conditions, insignificant flow obstructions, and negligible momentum within each zone [13]. The airflow rate between zones one and two, $\dot{V}_{12}$, is calculated with the orifice equation,

$$\dot{V}_{12} = AC_D\sqrt{\frac{2(P_1 - P_2)}{\rho}} \tag{2}$$

where A is the area of the opening, $P_1 - P_2$ is the static pressure difference between zones, and C_D is the dimensionless discharge coefficient. CoolVent shares many prominent features of most airflow network models such as a network of nodes, reliance on the Bernoulli equation, and use of a power-law function to calculate flow rates [9][13]. In light of these similarities, the improvements to CoolVent can be easily replicated in other airflow network models.

The improvements to CoolVent are made with empirical relationships that calculate pressure loss coefficients based on geometry and flow conditions. These relationships come from Idelchik's book, which defines a pressure loss coefficient ζ similar to Eq. 1 that calculates the total pressure loss based on a known bulk velocity [26]. However, this form of the pressure loss coefficient is inapplicable to CoolVent, which neglects momentum and thus relies only on static pressure to drive the flow [13]. Using the Bernoulli equation and definition of ζ, a ζ_{eff} is calculated based only on the static pressure difference.

$$\frac{P_1 - P_2}{\rho} + \frac{v_1^2 - v_2^2}{2} = \frac{\zeta v_1^2}{2} \tag{3}$$

Rearranging Eq. 3 in terms of the static pressure difference provides the definition of ζ_{eff}

$$P_1 - P_2 = \frac{\rho v_1^2}{2}\left[\zeta - \left(1 - \frac{v_2^2}{v_1^2}\right)\right] = \frac{\rho v_1^2}{2}\zeta_{eff} \tag{4}$$

where

$$\zeta_{eff} = \left[\zeta - \left(1 - \frac{v_2^2}{v_1^2}\right)\right] \tag{5}$$

This ζ_{eff} is converted to a discharge coefficient used in the orifice equation by equating the static pressure difference used to define both ζ_{eff} and C_D.

$$P_1 - P_2 = \frac{1}{C_D{}^2} \frac{\rho v^2}{2} = \zeta_{eff} \frac{\rho v^2}{2} \qquad (6)$$

Canceling similar terms and rearranging Eq. 6 yields the following relationship for C_D in terms of ζ_{eff}

$$C_D = \frac{1}{\sqrt{\zeta_{eff}}} \qquad (7)$$

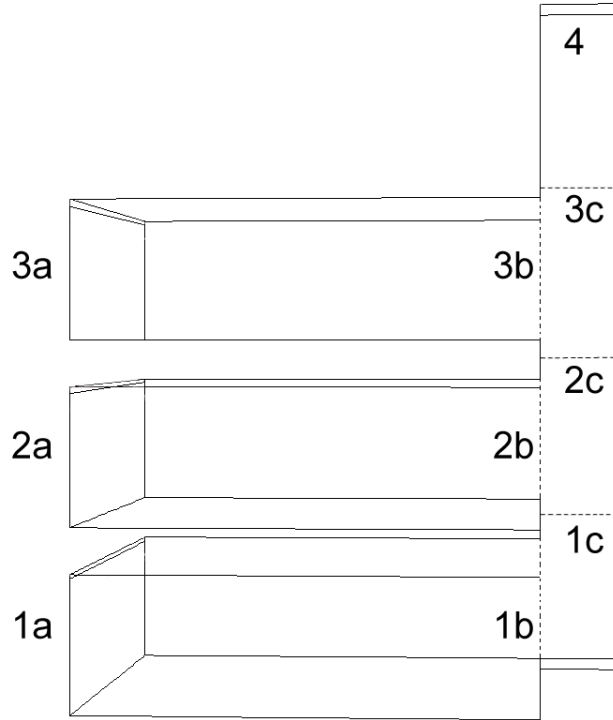Fig. 3 shows the three story office building with openings used in the CoolVent simulations.

Figure 3 – The same three story office building from CFD simulations is used in CoolVent, the geometry of which is shown here with labeled openings.

The value of ζ_{eff} for openings 1a, 2a, and 3a is 0.5, a constant value for the convergence of airflow from a large space to a small area [26]. The value of ζ_{eff} at opening 1b is calculated using Eq. 5 with the value of ζ coming from Idelchik's Diagram 6.6 for a 90^0 bend, which is summarized in Table 1 [26]. The basic geometry of the bend is shown in Fig. 4.
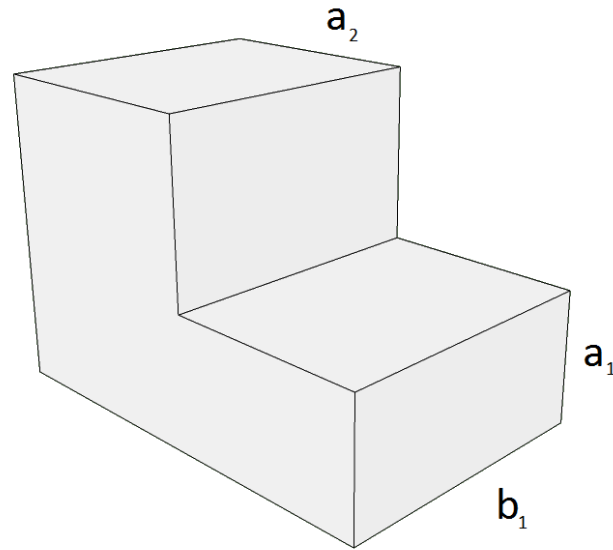
Figure 4 – Geometry of a 90^0 bend used to determine values of ζ from Idelchik's Diagram 6.6 [26].

Table 1 – Values of ζ obtained from Idelchik's Diagram 6.6 for a 90^0 bend shown in Fig. 4 [26].

	a_2/a_1			
b_1/a_1	0.6	1.0	1.4	2.0
0.25	1.76	1.24	1.09	1.06
1.0	1.70	1.02	0.95	0.84
4.0	1.46	0.81	0.76	0.66

Values of ζ_{eff} for openings 2b and 3b are calculated using relationships for the side branch of converging wyes at 90^0 and shown in Eq. 8 [26]. Values of ζ_{eff} for openings 1c and 2c are calculated using relationships for the straight passage through converging wyes at 90^0 and shown in Eq. 9 [26]. These two equations account for the momentum effects within the shaft and their impact on the flow through adjacent floors.

$$\zeta = 0.9 * \left(1 - \frac{\dot{V}_S}{\dot{V}_C}\right)\left[1 + \left(\frac{v_S}{v_C}\right)^2 - 2\left(1 - \frac{\dot{V}_S}{\dot{V}_C}\right)^2\right]\left(\frac{v_S}{v_C}\right)^2 \tag{8}$$

$$\zeta = \frac{1 - \left(1 - \frac{\dot{V}_S}{\dot{V}_C}\right)^2 - \left(1.4 - \frac{\dot{V}_S}{\dot{V}_C}\right)\left(\frac{\dot{V}_S}{\dot{V}_C}\right)^2}{\left(1 - \frac{\dot{V}_S}{\dot{V}_C}\right)^2} \tag{9}$$

7

To provide an example of how Eq. 5 is used to calculate ζ_{eff} using ζ from another relationship, ζ_{eff} is calculated for opening 2c.

$$\zeta_{eff2c} = \left[\frac{1-\left(1-\frac{\dot{V}_{3b}}{\dot{V}_{3c}}\right)^2 - \left(1.4-\frac{\dot{V}_{3b}}{\dot{V}_{3c}}\right)\left(\frac{\dot{V}_{3b}}{\dot{V}_{3c}}\right)^2}{\left(1-\frac{\dot{V}_{3b}}{\dot{V}_{3c}}\right)^2} \right] - \left(1 - \frac{v_{3c}^2}{v_{2c}^2}\right) \tag{10}$$

In Eq. 10, v_s and $\dot{V}_s$ are the bulk velocity and volumetric flow rate respectively through the opening from the adjacent floor; v_c and $\dot{V}_c$ are the bulk velocity and volumetric flow rate respectively through the chimney directly below the opening.

The value of ζ_{eff} for opening 4, the exhaust opening at the top of the chimney, is calculated with Eq. 5 where ζ is found using Eq. 11 for a sudden flow restriction [26].

$$\zeta = \left[0.707(1-\bar{f})^{0.375} + 1 - \bar{f}\right]^2 \frac{1}{\bar{f}^2} \tag{11}$$

In Eq. 11, $\bar{f}$ is the ratio of the exhaust area to the shaft cross sectional area. Frictional losses along the shaft are found to be negligible in these cases using the Darcy-Weisbach equation where $\zeta_{friction}$ is calculated as [27]

$$\zeta_{friction} = \frac{fL}{D_H}. \tag{12}$$

Where f is calculated using an empirical relationship developed by Haaland for the transitionally rough regime [27].

$$f = \left\{1.8log\left[\frac{6.9}{Re_d} + \left(\frac{\varepsilon}{3.7D_H}\right)^{1.11}\right]\right\}^{-2} \tag{13}$$

The largest value of $\zeta_{friction}$ is found at the top of the 2 m by 2 m shaft where the largest local velocities exist in the smallest cross-sectional area of the shaft. In this region, $\zeta_{friction} = 0.0153$, which is less than 2% of the pressure loss coefficient if friction is neglected. In narrower shafts, the pressure loss due to friction may be significant.

Both the original CoolVent, which represents typical airflow network models that neglect momentum effects, and the improved CoolVent, which accounts for momentum effects within the shaft, simulate the same three story office building modeled with CFD earlier in this paper. All geometric properties, heat gains, and ambient conditions from the CFD modeling are used in both versions of CoolVent to compare them to the CFD model.

4. Results

4.1 Results from Small Scale Experiment

The measured airflow rates for both 0.5 m by 0.25 m and 0.5 m by 0.5 m cases from the small scale experiments are presented in Table 2. The average volumetric flow rate of three trials is presented along with the standard deviation. Very little airflow, -0.0029 m^3/s, occurs through the upper duct in the 0.5 m by 0.5 m case, but when the shaft is reduced to 0.25 m by 0.5 m, it increases to 0.012 m^3/s. Similar airflow rates through the lower duct are observed in both cases. The average vertical velocity within the shaft can be found using the conservation of mass by dividing the airflow rate through the shaft by its cross sectional area. Directly above the lower duct, the average shaft velocity is 0.18 and 0.10 m/s for the 0.25 m by 0.5 m and 0.5 m by 0.5 m cases respectively. Directly above the middle, the average shaft velocity is 0.26 and 0.15 m/s for the 0.25 m by 0.5 m and 0.5 m by 0.50 m cases respectively. The average shaft velocity in the smaller 0.25 m by 0.5 m shaft is nearly twice as large as the average shaft velocity in the 0.5 m by 0.5 m shaft.

Results from the airflow visualization of the small scale experiment are presented in Fig. 5. Neutrally buoyant bubbles appear as white streaks against a black background. Some extraneous features of the setup are visible such as rectangular magnets, creases in the black felt, and reflections off acrylic paneling. The absence of bubble streaks in Fig. 5 3a) shows additional evidence of the slight reverse flow through the upper duct in the 0.5 m by 0.5 m case. Comparing Fig. 5 1a) with 1b) and 2a) with 2b) illustrates higher vertical shaft velocities in the smaller 0.25 m by 0.5 m case with longer vertical bubble streaks, which correspond to larger velocities because the same 1/4 s shutter speed is used for each photograph.

Although these results should not be directly compared to the CFD simulations of a full scale office building, they still provide a physical demonstration of the ejector effect by comparing the airflow through two ventilation shafts with a common exhaust area.

Table 2 –Averages of measured airflow rates from small scale experiments at each takeoff duct for both the 0.25 m by 0.5 m and 0.5 m by 0.5 m shafts. All values are reported in units [m^3/s] and the experimental error is +/- 0.0025 m^3/s.

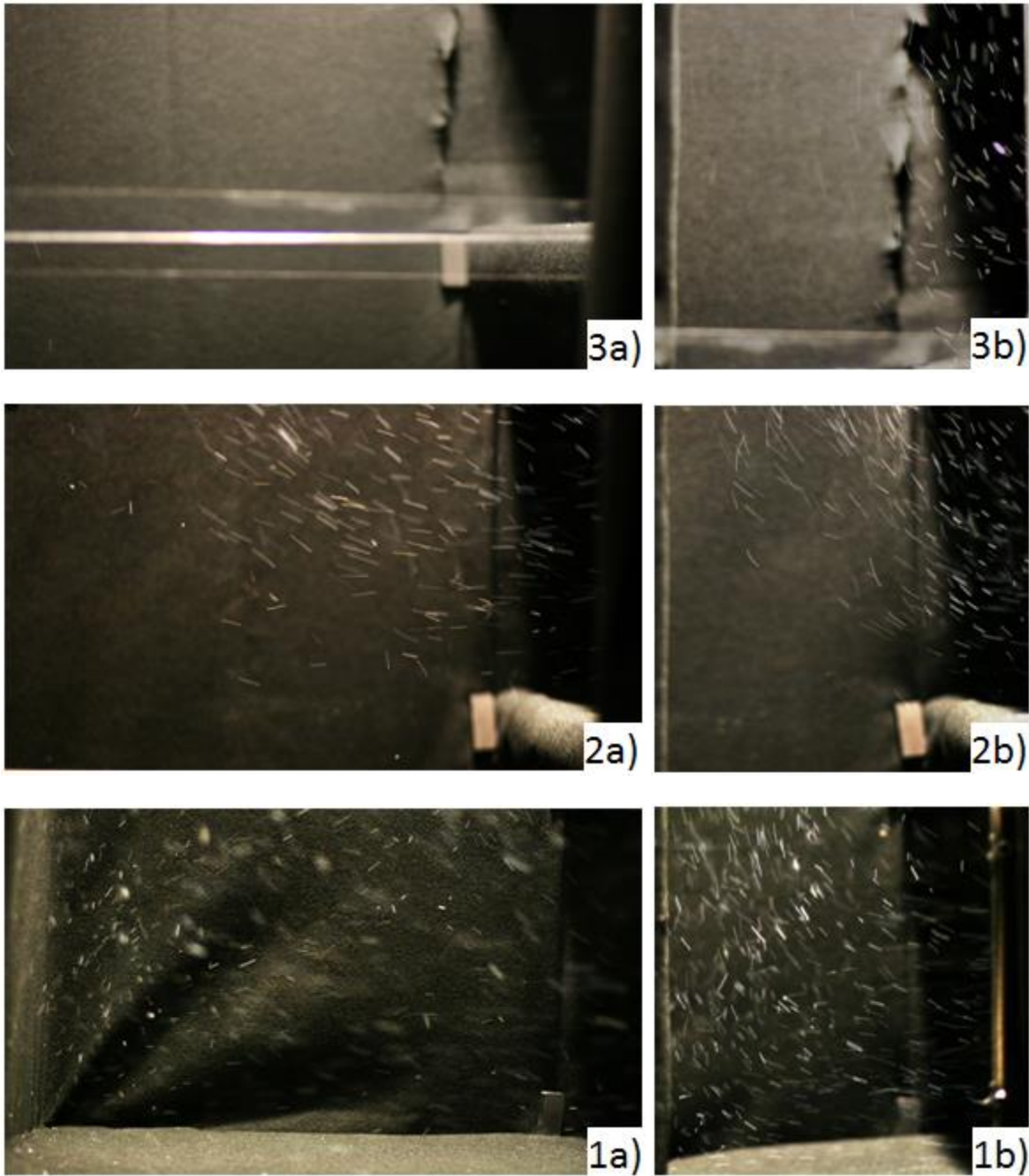| Takeoff Duct	0.25 m X 0.5 m	Std. Dev.	0.5 m x 0.5 m	Std. Dev.
Upper	0.012	0.00039	-0.0029	0.00027
Middle	0.0090	0.00063	0.011	0.0013
Lower	0.023	0.0035	0.026	0.0040

Figure 5 – Experimental airflow visualization of entrance from the 1a) lower duct into 0.5 m by 0.5 m shaft 1b) lower duct into 0.25 m by 0.5 m shaft 2a) middle duct into 0.5 m by 0.5 m shaft 2b) middle duct into 0.25 m by 0.5 m shaft 3a) upper duct into 0.5 m by 0.5 m shaft 3b) upper duct into 0.25 m by 0.5 m shaft. Air enters the shaft through each takeoff duct from the right side of the picture in all cases except 3a), where reverse flow occurs through the upper takeoff duct. The bright horizontal line in 3a) is an artifact of the joint between two acrylic sheets.

4.2 Results from CFD Simulations

Simulated flow rates through all three floors of the three story office building are presented in Fig. 6. Despite different geometries and heat loads, the results from the three story office building present a similar trend to those from the small scale duct experiment: higher flow rates through the upper floor are achieved with a smaller shaft. Temperature contours taken from the bisecting plane of the four sizes of ventilation shaft are presented in Fig. 7 and the temperature contour within the atrium is taken from the bisecting plane of the nearest two exhaust openings shown in Fig. 8. The locations of these planes are indicated in Fig. 2 for reference. Upper floor temperatures for the 2 m by 2 m shaft approach the upper limit of typical indoor temperatures, 27-28 ^{0}C. However, upper floor temperatures exceed comfortable levels in all other cases except the 10 m by 10 m atrium, where the same heat loads are distributed across nearly twice the floor area. The bulk temperature difference between the outdoor and shaft exhaust temperatures varies between 4.3 to 5.1 ^{0}C for the four different shaft sizes. Velocity fields are taken from the same locations and presented in Figs. 9 and 10 and reveal a similar trend to the one observed in the small scale duct experiment: higher shaft velocities are predicted in the smaller shafts. Additionally, Fig. 9 shows a bi-directional flow at the opening from the upper floor to the shaft for all cases except the 2 m by 2 m case in which unidirectional flow is predicted. Airflow rates from the CoolVent simulations are compared to the CFD results for the three story office building in Fig. 11.
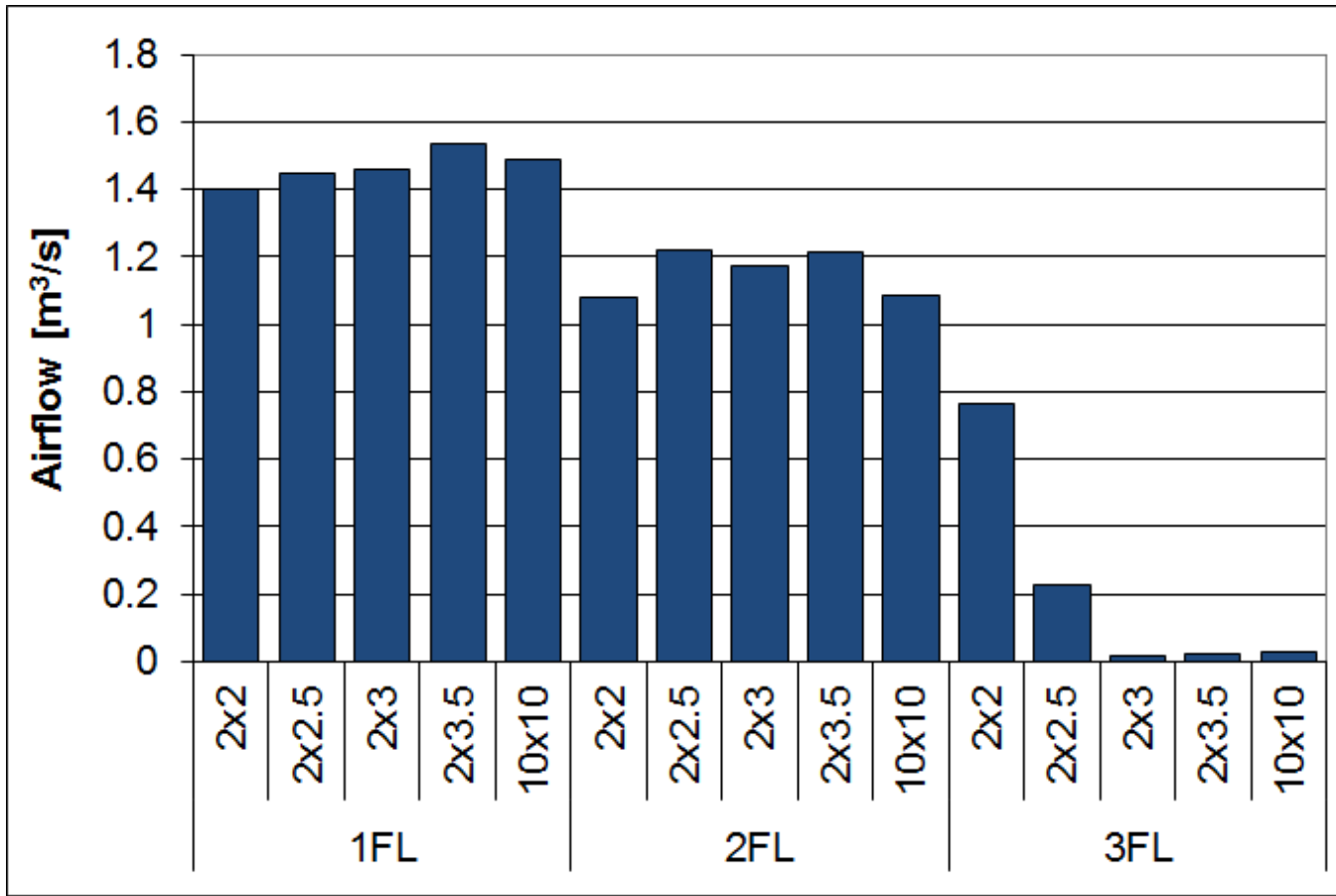

Figure 6 – CFD predicted flow rates for the three story office building for each of the five shaft cross sectional areas.
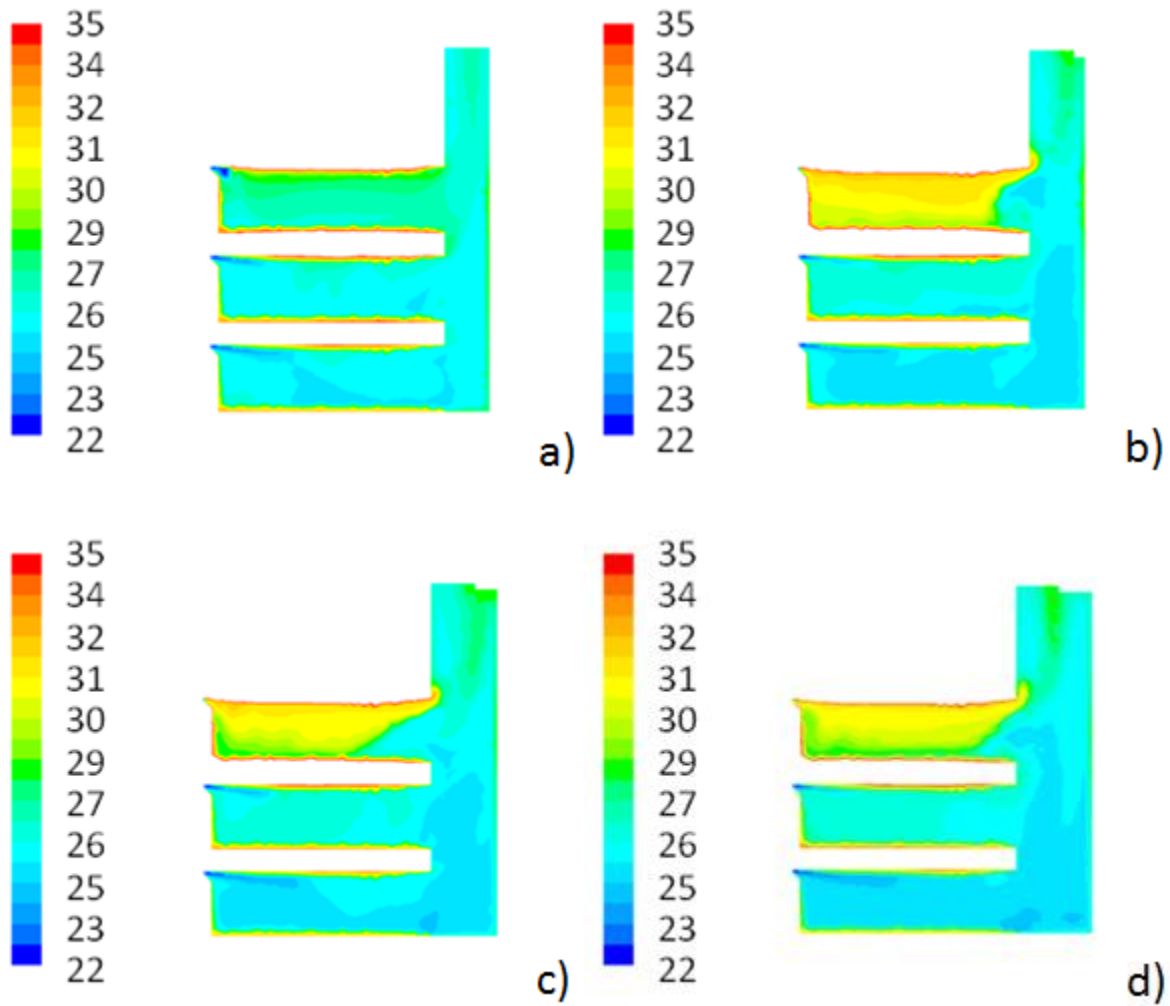
Figure 7 – CFD predicted temperature contour in ^{0}C taken from the bisecting plane of the a) 2 m by 2 m, b) 2.5 m by 2 m, c) 3 m by 2 m, and d) 3.5 m by 2 m shafts in the three story office building.
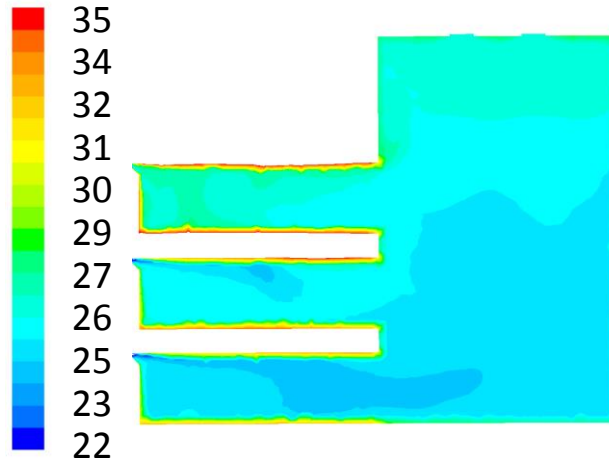
Figure 8 – CFD predicted temperature contour in ^{0}C of the 10 m by 10 m atrium taken from the bisecting plane of the two nearest exhaust openings in the atrium. While the total exhaust area is 4 m^2 like all other CFD simulated buildings, the opening from each floor to the atrium is 30 m^2 compared to 6 m^2 for the other cases.
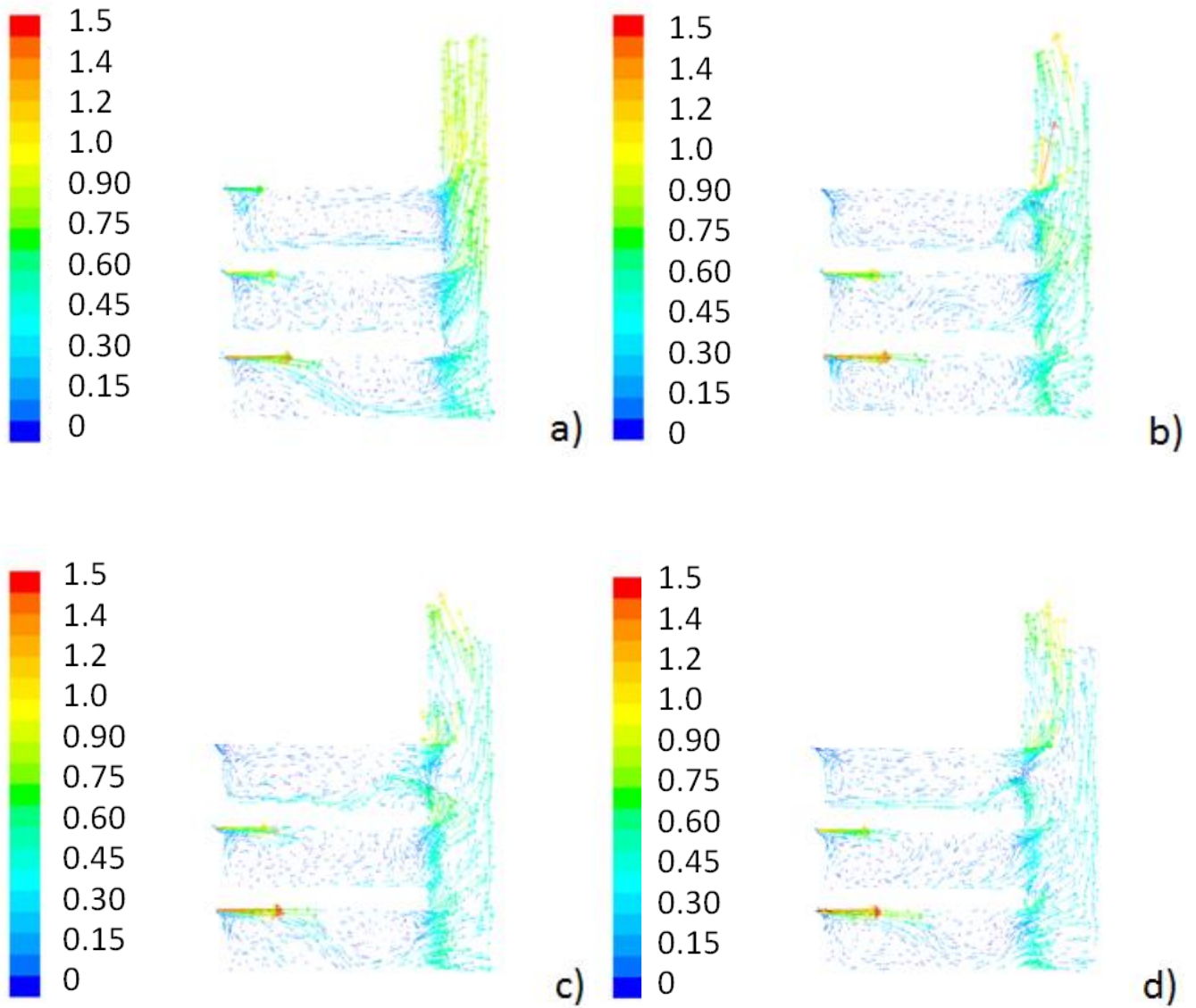
Figure 9 – CFD predicted velocity field in m/s taken from the bisecting plane of the a) 2 m by 2 m, b) 2.5 m by 2 m, c) 3 m by 2 m, and d) 3.5 m by 2 m shafts in the three story office building.
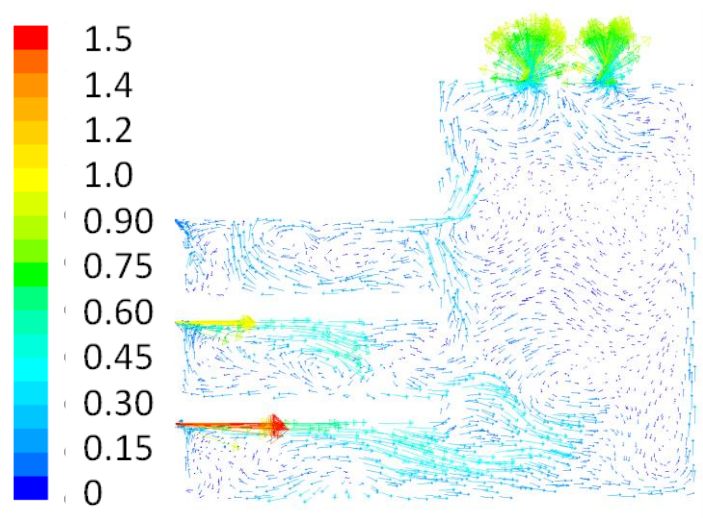
Figure 10 – CFD predicted velocity field in m/s of the 10 m by 10 m atrium taken from the bisecting plane of the two nearest exhaust openings in the atrium. While the total exhaust area is 4m^2 like all other CFD simulated buildings, the opening from each floor to the atrium is 30 m^2 compared to 6 m^2 for the other cases.
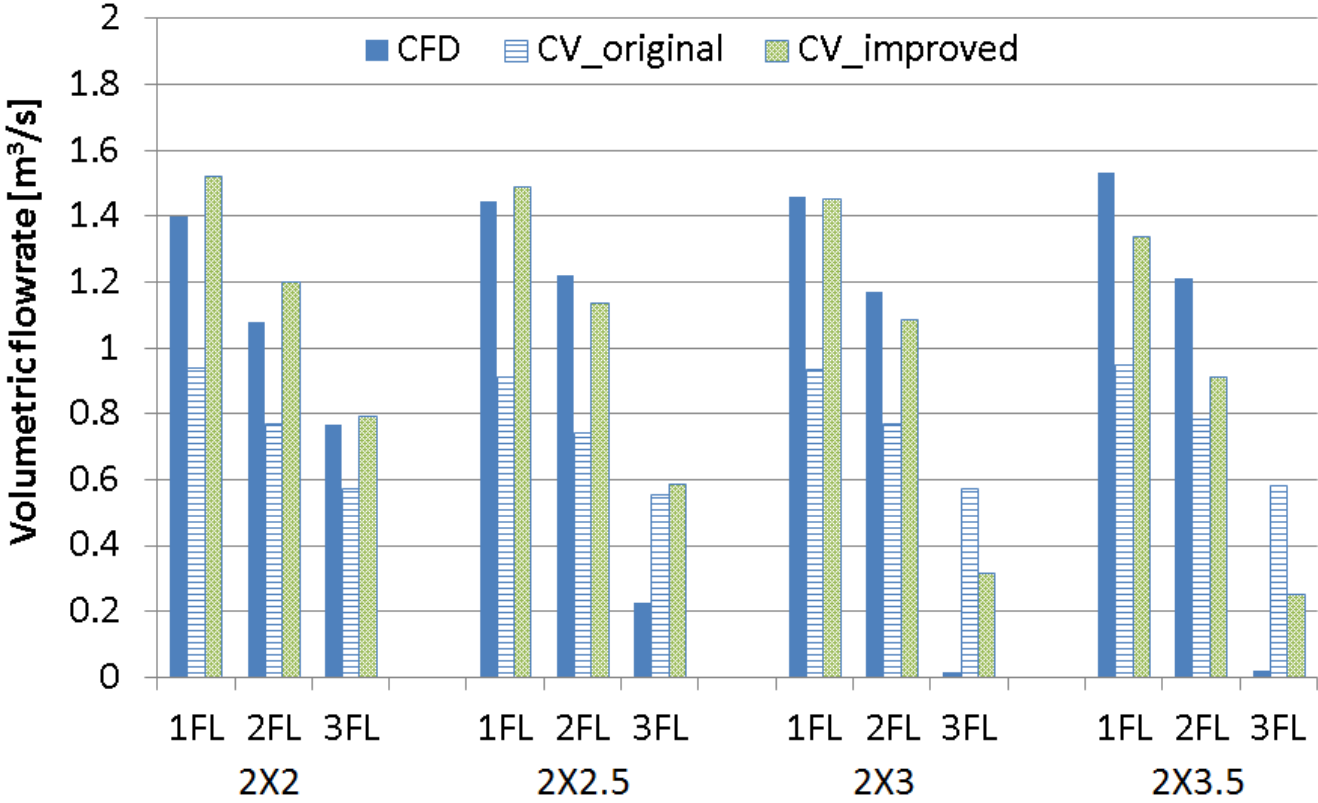

Figure 11 – Simulated airflow rates through the three story office building modeled with CFD, the original CoolVent, and an improved version of CoolVent. All four shaft sizes are considered and labeled on the horizontal axis.

5. Discussion

Measured flow rates from the small scale experiment presented in Table 2 show that essentially no airflow, 0.0029 m^3/s reverse flow, occurs through the upper takeoff duct in the 0.5 m by 0.5 m case. However, when the shaft area is halved to 0.5 m by 0.25 m, airflow through the upper duct, 0.012 m^3/s, surpasses the airflow through the middle duct, 0.0090 m^3/s, despite the larger height differential for the middle duct. This same dramatic increase in airflow through the upper floor is also predicted by the CFD simulations. Fig. 6 shows flow rates through the upper floor of the office building for larger chimney sizes of 3 m by 2 m and 3.5 m by 2 m, 0.0168 and 0.0224 m^3/s respectively, increase by more than an order of magnitude to 0.766 m^3/s when the shaft size is reduced to 2 m by 2 m. Natural ventilation is unsuitable for the third floor when a 3 m by 2 m shaft is used as indicated by the high temperatures shown in Fig. 7. By decreasing the shaft to 2 m by 2 m, the third floor temperature drops 3-4 ^{0}C. This scenario provides an example of how the ejector effect can be used to enable the use of buoyancy-driven natural ventilation in a building where it may otherwise be deemed ineffective. Although the small scale experiment and CFD simulations model two different geometries with different heat gains, they both illustrate how a smaller ventilation shaft can lead to higher flow rates through upper floors or takeoff ducts for a fixed exhaust area.

One explanation for this effect is that the airflow through the larger chimney must contract to be exhausted through the 2 m by 2 m outlet. This contraction introduces an additional pressure loss not experienced by the airflow in the 2 m by 2 m chimney case. However, if this were the sole explanation, the additional pressure loss should reduce the airflow through all three floors. Furthermore, it fails to account for the higher flow rate through the upper duct than the flow rate through the middle duct of the small scale experiment when the chimney size is reduced from 0.5 m to 0.25 m.

A more thorough explanation is provided by what has been called the ejector effect, which describes how increased vertical momentum within smaller shafts helps induce airflow through upper floors. The velocity fields presented in Figs. 9 and 10 illustrate this increased momentum and subsequent induced flow. Consider the velocity field for the 3 m by 2 m shaft in Fig. 9, in which air velocities in the shaft opposite the third floor are generally lower than 0.5 m/s. A clear reverse flow from lower floors into the third floor also exists. Comparing these two characteristics of the 3 m by 2 m shaft to the velocity field for the 2 m by 2 m case also shown in Fig. 9 reveals increased velocities in the 2 m by 2 m shaft opposite the third floor. These higher velocities increase the vertical momentum within the shaft and help induce flow through the third floor, where reverse flow no longer occurs. This same principle of using a stream of high momentum to induce flow through an adjacent space is commonly used in a jet pump, a schematic drawing of which is shown in Fig. 12. By the conservation of momentum, the increased momentum from the jet decreases the pressure at (1), which induces flow from reservoir (a) through the channel. Although no pump is used in the simulated office building, the smaller ventilation shaft creates higher local velocities, which increases the vertical momentum within the shaft enough to induce airflow through the third floor. Airflow visualization in the small scale experiment also suggests an increased vertical momentum in the smaller ventilation shaft. Longer vertical bubble streaks in the smaller shaft in Fig. 5 indicate increased vertical velocities. In the larger shaft, the airflow expands more as it enters the shaft and thus smaller vertical velocities are observed.
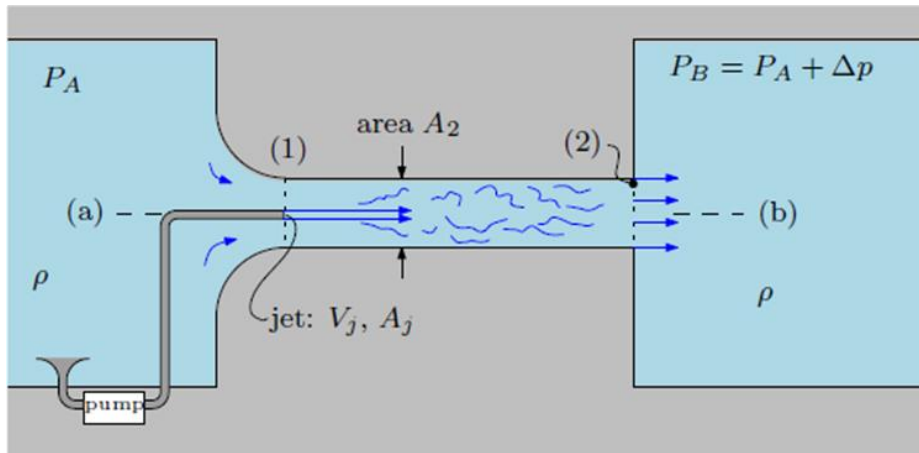
Figure 12 – Schematic drawing of a jet pump that uses a jet to increase momentum in a channel, thereby lowering the pressure at (1) and inducing flow from reservoir (a) through the channel.

As expected, results from the CoolVent simulations shown in Fig. 11 confirm that the original CoolVent predicts the same airflow rates for all four shaft sizes within the office building. Thus the significant impact of the ejector effect is not accounted for and the general trend of the CFD predicted flow rates is not matched. The original CoolVent under predicts the CFD values by nearly 40% for the first and second floors and drastically over predicts the airflow rate on the third floor for the 3.5 m by 2 m case. The improved CoolVent values agree much more closely with the CFD values on the first and second floors, agreeing to within 3% in some cases. The largest disagreement on these two floors is 19% for the first floor of the 3 m by 2 m case. Additionally, the improved CoolVent matches the trend of decreasing flow rate through the third floor as the shaft is expanded. Although the improved CoolVent over predicts the CFD value, it offers significant improvement over the original CoolVent by allowing designers to predict a trend rather than suggesting that an increased shaft area has no impact on the flow rate. This over prediction results from bi-directional flow at the opening from the upper floor to the shaft predicted by CFD. The empirical models incorporated into the improved CoolVent assume uni-directional flow at each opening, and thus do not account for the bi-directional flow. Fig. 9 shows this bi-directional flow in all cases but the 2 m by 2 m case, in which there is uni-directional flow. Consequently, the improved CoolVent predicts the third floor flow rate for the 2 m by 2 m case to within 4%, but over predicts the three other cases with bi-directional flow. Given the desire to only make improvements that are easily transferable to other airflow network models, the close agreement between the improved CoolVent and CFD on the first and second floors and the correct trend on the third floor provide significant and valuable improvements over the original CoolVent.

6. Conclusions

Buoyancy-driven natural ventilation in ventilation shafts is investigated with a small scale physical experiment within a duct and CFD simulations of an office building. For a fixed exhaust opening, smaller shafts lead to higher flow rates in upper floors of a multi-story building with a shared ventilation shaft. These higher flow rates are caused by increased vertical momentum within the smaller shafts that induce flow through upper floors, an effect referred to as the ejector effect. In the small scale duct, a 0.5 m by 0.5 m shaft leads to a slight reverse flow

of 0.0029 m^3/s through the upper floor. Holding all other parameters constant and reducing the shaft to 0.25 m by 0.5 m leads to a flow rate of 0.012 m^3/s through the upper floor. In the CFD simulations of a three story office building, this same pattern is observed. A 3 m by 2 m shaft leads to a flow rate of 0.0168 m^3/s through the third floor, while the reduced shaft of 2 m by 2 m leads to a flow rate of 0.766 m^3/s through the same floor. This increased airflow rate from the ejector effect can allow natural ventilation to be used in buildings where it may otherwise have been deemed inappropriate, as in the simulated three story office building with a 3 m by 2 m ventilation shaft.

Most airflow network models assume negligible air momentum and fail to account for the ejector effect. Results from the original CoolVent, an MIT-developed airflow network model, demonstrate the inaccuracies this assumption can introduce when ventilation shafts are used, in which momentum effects can be significant. To improve airflow network models, an empirical model is incorporated into CoolVent that accounts for some of the momentum effects within ventilation shafts. The improved CoolVent is shown to more accurately model the three story office building simulated with CFD. Although these improvements leave room for further accuracy gains, especially in modeling bi-directional flow, they offer significant gains over current models that neglect air momentum. Improvements to CoolVent are designed to be easily transferable to most airflow network models to better account for the ejector effect in ventilation shafts and promote their use in buoyancy driven natural ventilation systems.

In addition to enhancing the ability to model bi-driectional flow in airflow network models, future work should focus on optimizing the shaft cross sectional area to maximize the ejector effect while maintaining acceptable frictional pressure losses. As the shaft cross sectional area is reduced, local velocities are increased, which increases the vertical momentum within the shaft and further induces airflow through upper floors. However, higher velocities along the shaft walls also lead to larger frictional losses within the shaft.

More research is also needed to better isolate the effect of the exhaust geometry from the ejector effect. The shaft geometry investigated in the current work couples an increased pressure drop from a sudden reduction in cross-sectional area at the exhaust for large shafts with a decrease in vertical momentum due to lower local velocities within the shaft. Although the same exhaust opening is used, except for the atrium configuration, the transition from the shaft to the exhaust opening should be more uniform in future work to better isolate the ejector effect.

7. Acknowledgements

References

 [1] Liu P-C, Lin H-T & Chou J-C. Evaluation of buoyancy-driven ventilation in atrium buildings using computational fluid dynamics and reduced-scale air model. Building and Environment 2009; 44(9):1970-79.

[2] Walker C, Tan G, Glicksman L. Reduced-scale building model and numerical investigations to buoyancy-driven natural ventilation. Energy and Buildings 2011;43(9):2404-13.

 [3] Walker C. Methodology for the Evaluation of Natural Ventilation in Buildings Using a Reduced-Scale Air Model. PhD thesis, Massachusetts Institute of Technology, 2006.

[4] Rundle CA, Lightstone MF, Oosthuizen P, Karava P, & Mouriki E, 2011. Validation of computational fluid dynamics simulations for atria geometries. Building and Environment 2011;46(7):1343-53.

[5] Ray S, Glicksman LR, & Fukuda M. Case study of hybrid ventilation system with exhaust shafts. Presented at Roomvent 2011, Trondheim, Norway, June 2011.

 [6] Carrilho da Graca D, Linden P, & Brook M. Design of the natural ventilation system for the New San Diego Children's Museum. Presented at the Ninth International IBPSA Conference, Montreal, Canada, August 2005.

[7] Short CA & Lomas KJ. Exploiting a hybrid environmental design strategy in a US continental climate. Building Research and Information 2007;35(2):119-43.

[8] Cook M & Short CA. Natural ventilation and low energy cooling of large, non-domestic buildings - four case studies. International Journal of Ventilation 2005;3(4):283-94.

[9] Qingyan C. Ventilation performance prediction for buildings: A method overview and recent applications. Building and Environment 2009;44(4):848-58.

[10] EnergyPlus 7.1 Engineering Reference. US Department of Energy, 2012.

[11] TRNSYS 17, TRNSYS A transient systems simulation program (2012) http://sel.me.wisc.edu/trnsys

[12] Energy Systems Research Unit (ESRU) ESP – A building and plant simulation system, User Guide 1998, ESRU, University of Strathclyde, Glasgow.

[13] Menchaca-Brandan M-A & Glicksman L. Coolvent: A multizone airow and thermal analysis simulator for natural ventilation in buildings. Presented at Simbuild 2008 IBPSA-USA National Conference, Berkley, USA, August 2008.

[14] Etheridge D & Sandberg M. *Building Ventilation: Theory and Measurement*, John Wiley & Sons, 1996.

[15] Ding W, Hasemi Y, & Yamada T. Natural ventilation performance of a double-skin facade with a solar chimney. Energy and Buildings 2005;37(4):411-18.

[16] ASHRAE Standard 111-2008: Measurement, Testing, Adjusting, and Balancing of Building HVAC Systems. ASHRAE, Atlanta, GA, 2008.

[17] Graywolf Sensing Solutions. AdvancedSense Product Specifications, 2011.

[18] SAI Model 5 Console. http://www.sageaction.com/

[19] Sun Y & Zhang Y. Development of a stereoscopic particle image velocimetry system for full-scale room airflow studies, part II: experimental setup, ASHRAE Transactions 2003;109 (part 2).

[20] Zhang Z, ZhangW, Zhai Z, Chen Q. Evaluation of various turbulence models in predicting airflow and turbulence in enclosed environments by CFD: part 2 – comparison with experimental data from literature. HVAC&R Research 2007;13(6):871–86.

[21] Yuan CS. The effect of building shape modification on wind pressure differences for cross-ventilation of a low-rise building. International Journal of Ventilation 2007;6(2):167–76.

[22] Kuznik F, Rusaou_en G, Brau J. Experimental and numerical study of a full scale ventilated enclosure: comparison of four two equations closure turbulence models. Building and Environment 2007;42(3):1043–53.

[23] Tapsoba M, Moureh J, Flick D. Airflow patterns inside slotted obstacles in a ventilated enclosure. Computers and Fluids 2007;36(5):935–48.

[24] Rohdin P, Moshfegh B. Numerical predictions of indoor climate in large industrial premises. A comparison between different k–e models supported by field measurements. Building and Environment 2007;42(11):3872–82.

[25] Zhao L, Wang X, Zhang Y, Riskowski GL. Analysis of airflow in a full-scale room with non-isothermal jet ventilation using PTV techniques. ASHRAE Transactions 2007;113(Part 1):414–25.

[26] Idelchik IE. Handbook of Hydraulic Resistance 3rd ed. Jaico Publishing House, Mumbai, 2001.

[27] White FM. *Fluid Mechanics*. The McGraw-Hill Companies, 1999.